Building and Environment 250 (2024) 111113

Contents lists available at ScienceDirect

Building and Environment

journal homepage: www.elsevier.com/locate/buildenv

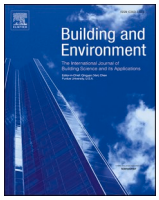

Microclimatic implications of a large-scale green roof and high-rise redevelopment in New York City

Bita Alizadehtazi, Julian Stolper, Katelyn Singh, Franco A. Montalto *

Department of Civil, Architectural & Environmental Engineering, Drexel University, 3141 Chestnut Street, Philadelphia, PA, 19104, USA

ARTICLE INFO

Keywords:
Green roof
Urban heat island
ENVI-met
Microclimate
Urban climate
Urban sustainability

ABSTRACT

This paper quantifies the impacts of the Jacob K. Javits Convention Center (JJCC) green roof and the nearby redevelopment of Hudson Yards (Midtown West, Manhattan, New York City, NY) on the local microclimate. The analysis was performed using ENVI-met, a grid based, three-dimensional (3D) computational fluid dynamics model commonly used to simulate surface-plant-air interactions in urban settings. Using air temperature, relative humidity, and wind speed and direction measured onsite on July 22, 2014, a total of six simulations were run, comprising three different stages of redevelopment (e.g., in 2014, 2018, and 2021), with and without the JJCC green roof in place. Under the simulated climate conditions, the green roof reduced air temperature over the no-green roof (NoGR) condition, primarily on the north side of the JJCC. However, because of the nearby redevelopment, the cooling benefit provided by the roof decreased slightly over time. For example, at 1:00 p.m. the air temperature dropped from 0.75 K at roof level in 2014, to 0.65 K and 0.64 K in 2018 and 2021, respectively. Similarly, though to a lesser extent, the same trends were evident in the simulations at pedestrian level. The redevelopment of Hudson Yards reduced the sky view factor (SVF) and provided shading during the day, reducing daytime mean radiant temperature (MRT). However, the same buildings raised nighttime MRT. Together, the study provides insights into the growing understanding of how green roofs can impact the microclimate of complex urban environments.

1. Introduction

It is well known that urban areas can experience higher ambient air temperatures than nearby rural areas [1], with measured differences of between 0.4 and 11 K [2]. During heat waves [3], urban heat islands (UHIs) can be more extreme [4], negatively impacting the health and well-being of the urban population [5,6]. As reviewed by Tzavali et al. [7], the intensity of the UHI is determined by latitude, elevation, climate, land use, surface morphology, proximity to water bodies, urban "canyons", degree of urbanization, vegetative cover, building density, energy consumption, road traffic, air pollution, impervious surfaces [8], albedo [9], and other emergent characteristics of urban morphology. Though UHIs are, and have been, of keen interest to a wide range of researchers [10], there is increasing interest in intra-urban and intra-neighborhood differences and, in particular, factors that determine outdoor thermal exposure and comfort [11].

Measurements correlating the intensity of the UHI to specific urban forms are generally limited and complicated by site-specific morphological differences [12]. Direct comparison of measurements is also complicated by differences in monitoring techniques; the season, duration, and frequency of measurements; the methodology used to select the rural reference location; and a lack of specificity regarding the subject site and surrounding land cover [2,13,14].

Most measurement campaigns highlight spatial differences in surface temperature, with less emphasis placed on the spatiotemporal heterogeneity in air temperature [15], and related factors. With air temperature, metrics such as the sky view factor (SVF) [16], the ratio of free sky visible from a single point to the total sky area, and mean radiant temperature (MRT), a measure of the exchange of radiant heat between a human and her/his environment, are now recognized as key determinants of urban microclimate and related thermal comfort [17].

Modeling tools can also be used to explore the complex interplay of site-specific factors in determining UHI, and thermal comfort. ENVI-met [18] is a grid based, three-dimensional (3D) computational fluid dynamics model used widely to predict micro-climatological conditions inside an urban canopy [19,20]. The model can be used to isolate specific differences under different morphological scenarios [21] contributing to understanding of how specific urban morphological

* Corresponding author.
E-mail address: fam26@drexel.edu (F.A. Montalto).

https://doi.org/10.1016/j.buildenv.2023.111113
Received 31 August 2023; Received in revised form 22 November 2023; Accepted 11 December 2023
Available online 13 December 2023

characteristics interact to generate the UHI. This kind of understanding is crucial to efforts to develop urban planning and infrastructure designs that can build adaptive capacity and mitigate the impacts of climate change.

As part of a broader effort to study urban interactions between soil, water, climate, and vegetation that determine the ability of nature-based infrastructure strategies to advance sustainability and resilience in cities [22–31], this study simulates the impacts of a green roof on the urban microclimate in a redeveloping urban landscape. The research is situated in and around Hudson Yards, on the west side of Manhattan, New York City, New York, location of the most expensive real-estate development in US history [32]. At completion, this $25 billion, 11.31-ha redevelopment project will include 1.67 million square meters of real estate, including multiple high-rise buildings and 5.7 ha of public space. Hudson Yards is an appropriate location to study the dynamic interplay between urban development and nature-based adaptation strategies because it also includes the Jacob Javits Convention Center (JJCC), host to the second largest, extensive green roof in the United States.

A growing body of work attempts to model the microclimatic impacts of green roofs in densely developed urban landscapes. Although green roofs can reduce the overlying air temperature, their ability to cool air at pedestrian level is less pronounced, and reduced with building height [33]. Tsoka et al. [34] reviewed microclimate simulations performed using ENVI-met that evaluated the impact of green roofs on urban microclimate. They reported maximum simulated cooling potential of green roofs at pedestrian-level ranging between 0.1 °C and 1.70 °C, with a median cooling of ~0.30 °C. Focusing on an industrial district in Italy, Ciacci et al. [35] found that an extensive green roof could reduce air temperature by up to 1.5 °C. Liu et al. [36] found that the Pedestrian Cooling Intensity (PCI) was highest when green roofs were installed on low-rise buildings. Focusing on a college campus, Zheng et al. [37] found that pedestrian-level cooling benefits of an extensive green roof amounted to 0.29 °C. Iaria and Susca [38] found that the ability of an extensive green roof to mitigate the UHI decreased with increasing building height, becoming negligible for green roofs that were 40 m over the surface. Focusing on a residential district, Feng et al. [39] found that pedestrian-level cooling intensity became insignificant when roof height reached 50 m. The only paper focusing on green roofs in an urban landscape characterized by high-rise development was Balany et al. [40] who found that green roofs provided a small (<0.47 °C) temperature reduction in the surrounding area, with no noticeable improvement in the level of thermal perception.

The research presented here contributes to this sparse but evolving body of work by attempting to isolate the impact of the green roof from that of the surrounding buildings in a densely developed, temperate climate. Prior to the development of the Hudson Yards construction and when only the north portion of the JJCC roof had been greened, Alvizuri et al. [41] investigated thermal buffering of the JJCC green roof using infrared imaging. Comparing the north green roof to the black bitumen roof still located on the south portion of the building, the authors reported that the exterior surface temperature of the green roof was on average 16.9 °C cooler than the black bitumen roof, and was also 5–10 °C cooler than adjacent sidewalk surfaces. Smalls-Mantey and Montalto [28] also explored the microclimate and energy fluxes above different surfaces on and around the JJCC green roof, before and after installation. During construction, the air temperature above the southern black bitumen roof was higher than the air temperature above the north green roof, with a maximum daytime air temperature difference of 1.80 °C. In August 2013, the measured, monthly median air temperature over the black roof was about 0.4 °C greater than measured over the green roof. After the southern roof was greened, its air temperature remained slightly higher than over north green roof, suggesting that some of the observed differences may have been due to morphological factors beyond the roof boundaries. Smalls-Mantey and Montalto [28] did not observe street-level cooling effect of the JJCC green roof. The observed temperature differences on and around the JJCC green roof were similar to those modeled at other locations.

This study extends the work of [28,41] at the JJCC green roof using ENVI-met. Specifically, this study simulates microclimate conditions for six scenarios: a) 2014 environment with no green roof (baseline), b) 2014 environment with green roof, c) 2018 environment with partial development and green roof, d) 2018 environment with partial development and no green roof, e) 2021 environment with full development and green roof, and f) 2021 environment with full development and no green roof. The goal is to use the model to investigate the complex interactions between the green roof and nearby high-rise buildings in determining the local microclimate.

2. Materials and methods

2.1. Case study site description

The JJCC green roof is located between 11th and 12th Avenues, and between W 34th and W 40th streets, on the west side of Manhattan, New York City, New York (Fig. 1). It is bordered to the south and east by Hudson Yards (Fig. 1), the most expensive mixed-use private real estate development in history [32,42], which broke ground a few years after the installation of the JJCC green roof.

The JJCC green roof is extensive and 27,316 m^2 in total area, with the North Green Roof (NGR) and South Green Roof (SGR) separated by a taller section of the building. Construction was completed in the spring of 2014. In section, the green roof consists of a Xero Flor XF301 + XT extensive system, with a pre-vegetated sedum mat installed on top of 1.5–5 cm of growing medium, a retention fleece layer, a drainage layer, and a root barrier, as described in detail in Alvizuri, Cataldo, Smalls-Mantey and Montalto [41].

2.2. Microclimate simulation process

2.2.1. ENVI-met model description

Microclimate simulations of the JJCC green roof were performed using ENVI-met [18] V4.4.4, a grid based, three-dimensional (3D), computational fluid dynamics model used to simulate surface-plant-air interaction in urban settings. ENVI-met performs unsteady computations by solving the Reynolds-averaged Navier-Stokes equations. The general workflow using ENVI-met can be found in relevant papers [43,44]. The model simulations are initiated using a one-dimensional boundary condition that is subsequently subjected to continuous forcing. The geographical setting and 3D model domain were developed by defining surfaces with soil and vegetation, and identifying buildings, and characterizing the topography. The simulation file was used to specify the time of day, simulation period, and meteorological conditions used in the analysis.

2.2.2. Model scenarios

To evaluate the impacts of the JJCC green roof and the Hudson Yards development on the local microclimate, simulations of the same geographic area under the same simple climatic forcing were undertaken at different stages of simulated Hudson Yards redevelopment. These morphological stages roughly coincide with redevelopment progress in 2014, 2018, 2021 (Table 1, Fig. 2). For each stage of these three stages of redevelopment, one simulation was performed with the green roof (GR) in place, and one assuming a more conventional, no-green roof (NoGR) condition. Note that when the research was initiated, the Hudson Yards project was projected to be complete by 2021. However, the project was delayed and not complete in 2021. Nonetheless, the "2021" model assumes redevelopment was complete (e.g., it represents the proposed final construction). We also note that, since initiation of this research, the Javits Center has added a building to its north, with a rooftop farm, orchard, and food forest. Because designs for this project were not available when this research began, it was not included in the current modeling.

Fig. 1. Plan view of Jacob K. Javits Convention Center (JJCC) and Hudson Yards study area in New York City, New York (source: Google maps 2021); orange circles show weather station located on North Green Roof (NGR), South Green Roof (SGR), and at pedestrian-level at 11th AVE, red stars show ENVI-met model receptor locations on NGR, SGR, and pedestrian-level at 11th Ave. Table 3 provides additional information about the weather stations, including their elevation. (For interpretation of the references to color in this figure legend, the reader is referred to the Web version of this article.)

Table 1
Model scenarios description.

Name	Description
2014	The JJCC green roof is complete, and on-site climatic monitoring initiated. The Hudson Yards project had not yet begun.
2018	The Hudson Yards project was partially complete, consisting of three completed buildings, two partially constructed buildings, and three empty lots.
2021	The Hudson Yards project is assumed to be fully complete. All completed buildings from the 2018 model are included from the 2018 environment, while partially completed buildings are brought to their terminal height and 3 additional buildings added to the empty lots.

Note: with the exception of the Hudson Yards development south and east of JJCC, all of the elements were kept constant for all models.

2.2.3. ENVI-met model design and parameter selection

In each model, the horizonal (x, y) dimensions of each grid cell were set to 6 m × 6 m, resulting in a total horizontal modeled area of 894 × 840 m (Table 2). The standard z-dimension resolution was 2 m. However, as recommended by ENVI-met, the domain height was scaled to at least twice as high as the tallest building in each simulation to prevent the top boundary from distorting the results around the buildings of interest [45]. In the 2014 scenario, JJCC was the tallest building in the model domain, resulting in a total model domain height of 82 m. Because the buildings introduced in the Hudson Yard redevelopment project are much higher, the 2018 and 2021 models used a domain height of 740.08 m. However, to reduce the number of vertical cells, the model was telescoped [20,46]. That is, the first 82 m of height used the standard 2 m grid resolution, while the vertical length of each additional grid cell above that threshold was increased by 10 % (Table 2). Telescoping allowed the larger models to obtain the desired vertical height while minimizing computational complexity in grids outside the area of interest.

2.2.4. 2014 model domain

The JJCC is incised into a sloping terrain that is higher on the east side of the building and lower to the west near the Hudson River. The building is also separated from the street by an open space roughly at street elevation on the west side of the building. The roof of the building contains complex shapes and towers that were represented as accurately as possible in the model given its grid resolution. The green roof surface is 17 m above the street elevation on its east side, but to account for the sloping terrain, the model assumes it to be 21 m above the average perimeter surface elevation. In addition, some of the irregularities in the

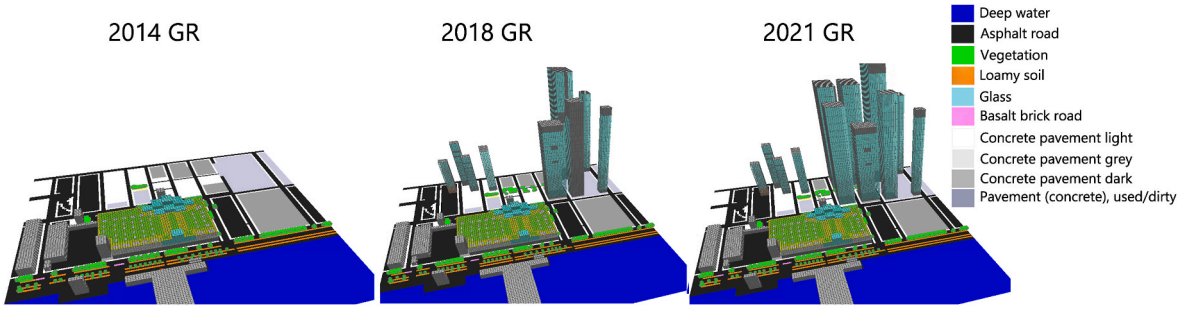

Fig. 2. Simulation models for GR 2014 (left), GR 2018 (middle), and GR 2021(right) scenarios. Note: the only difference between GR and NoGR scenarios are placement of JJCC green roof. (For interpretation of the references to color in this figure legend, the reader is referred to the Web version of this article.)

Table 2
Properties of model domain, model parameters, and meteorological initial conditions.

Parameter	2014	2018	2021
Spatial resolution	6 × 6 × 2 m	6 × 6 × 2 m w/10 % telescoping after 82 m	6 × 6 × 2 m w/10 % telescoping after 82 m
Domain size	894 × 840 × 82 m	894 × 840 × 740.08 m	894 × 840 × 740.08 m
Model rotation from north	29°	29°	29°
Location coordinates[a]	40.76° N 74° W	40.76° N 74° W	40.76° N 74° W
Start time	3:00 a.m.	3:00 a.m.	3:00 a.m.
Simulation duration	24 h	24 h	24 h
Roughness length [40, 47]	2	2	2
Wind direction (avg)	183.00°	183.00°	183.00°
Wind speed (avg)	1.81 (m/s)	1.81 (m/s)	1.81 (m/s)
Minimum/maximum air temperature[b]	18.35 °C/ 32.84 °C	18.35 °C/ 32.84 °C	18.35 °C/ 32.84 °C
Minimum/maximum relative humidity[b]	46.10 %/81.09 %	46.10 %/81.09 %	46.10 %/81.09 %
Soil upper layer (0–20 cm)[c] moisture content/initial temperature	70 %/19.85 °C	70 %/19.85 °C	70 %/19.85 °C
Soil middle layer (20–50 cm)[c] moisture content/ initial temperature	75 %/19.85 °C	75 %/19.85 °C	75 %/19.85 °C
Soil deep layer (below 50)[c] moisture content/initial temperature	75 %/19.85 °C	75 %/19.85 °C	75 %/19.85 °C
Metrological boundary conditions	Simple forcing	Simple forcing	Simple forcing

[a] The location coordinates of the model allow the software to appropriately simulate the Sun's path and location on the sky, depending on the time of year.
[b] Table depicts the minimum and maximum values used for simple forcing of the model. The full time series data is provided in Table S5.
[c] ENVI-met default values.

Table 3
Onsite climate station and specifications.

Measured parameter	Equipment manufacture/ model	Specifications	Approx. height over street (m)
Logger	Campbell Scientific, Inc. CR1000	Logged at 5 min intervals	–
Air temperature and relative humidity	Campbell Scientific, Inc. CS215	Air temperature: ±0.3 °C relative humidity: ±4 %	On roof ~24 11th Ave ~3
Wind speed & direction	Young Company Model 5103 Wind Sentry Anemometer	Anemometer: ±0.5 m/s Vane: ±5°	On roof ~24 11th Ave ~3

roof top surfaces have not been represented in the model.

Using Google Earth, other local buildings such as the Port Authority Bus Terminal, a City-owned tow pound, the Lincoln Tunnel exhaust vents, and a few other smaller buildings were represented in the base, No-GR model (Fig. 1). The time-machine function of Google Earth was used to approximate their condition at different time periods. Surfaces were approximated as concrete, pavement, and soil as appropriate. Slightly different concrete, brick, and pavement types were used to differentiate roads, sidewalks, and construction areas. For these areas, default ENVI-met materials were used. Default 'loamy soil' was used in ground areas that hosted vegetation and street trees. Default "deep water" characteristics were assigned to the Hudson River. The characteristics of the soil, pavement, and deep water were kept constant throughout all models and simulations. All buildings outside of JJCC placed in the 2014 model were built with a default concrete wall with moderate insulation for simplification of the model area. The JJCC building itself was constructed with more detail, derived from its engineering drawings (Supplementary Materials Table S1). Vegetation was inserted into areas around JJCC, with street tree types derived from a NYC Parks website [48].

Once this NoGR base model was completed, a GR base model was created by replacing the black roof with a soil/vegetation surface to best match the properties of the actual design (e.g., Tables S2 and S3).

2.2.5. 2018 model domain

The 2018 models (GR and NoGR) were built by creating a copy of the 2014 model to keep the base conditions consistent. Historical imagery from Google Earth was again used to estimate the actual state of redevelopment in the Summer of 2018. The heights of these buildings were estimated using the elevation indicator in Google Earth, which was found to accurately estimate the heights of fully built buildings in 2021 when compared to engineering plans [49]. The materials used for these buildings are listed in Table S4. The 2018 Hudson Yards development included street trees in three parts (each approximately 55 × 45 m), collectively known as "Hudson Park". The GR model was created as described above.

2.2.6. 2021 model domain

The No-GR 2021 model was a replica of the 2018 model with some buildings added and/or completed, to reflect project completion per the design drawings. The final building heights were determined from open access building plans for the buildings, available online [50]. Again, the GR model was created from the No-GR model as described above.

2.2.7. Simulation setup and initialization

Once all the 3D models were created and detailed, they were added to the simulation file, executed in the ENVI-met Core application. A day in 2014 with minimum and maximum values of air temperature (18.35 °C and 32.84 °C, respectively) and relative humidity (46.10 % and 81.09 %, respectively) was selected for the simulation (Table 2). The full hourly time series of this data is included in Table S5. For reference, a local weather station (40.76 °N, 73.86 °W) reports a maximum monthly average temperature of 28.27 °C and relative humidity of 85.30 % for July, suggesting this day is close to a monthly high. This particular day in 2014 was also selected because it is the study baseline year (before Hudson Yards development) and because on-site monitoring data was available for model calibration, as discussed below. Each simulation lasted 24 h, beginning at 3:00 a.m. to allow the model to warm up for 10 h. Nesting grids added a significant computational time to the simulations. As an alternative approach to ensuring border stability in the models, the first three grid systems were left void of buildings.

2.2.8. Field measurements

Many sensors were installed on JJCC as part of a broader effort to study its energy and water balance. This study utilizes data from the onsite weather station (Table 3). Climatic data measured at the NGR weather station on July 22, 2014, was used for model initialization. The average wind speed and direction from that day was applied to the domain boundary to force the model and were kept constant across all the models (Table 2). Initially, the air temperature and relative humidity (RH) used at the border were derived from the NGR weather station time series. These values were later modified as described below to create the model boundary condition.

2.3. ENVI-met simulation calibration, validations, and goodness of fit

Virtual nodes known as receptors can be placed at various points in

the model for calibration and analysis of the model results. A timeseries of simulation data was generated for each receptor node. Receptors were placed in the approximate location of the other on-site weather stations (see orange circles and red stars in Fig. 1) to validate the model results, and in other points of interest to the comparative analysis of the model results.

Calibration of the 2014 GR model involved comparing simulated estimates of air temperature and relative humidity at the NGR reactor with the measured observations from the NGR weather station. Initially, the ENVI-met receptor results were temporally out of phase with the observed data. This lag was expected, as the original boundary forcing data was derived from the hourly observed data collected on the NGR. To remove this lag, the final model forcing data was computed by calculating the simulated temporal offset between the model boundary and the NGR receptor, which was then used as the model boundary condition. With this adjusted boundary condition and rerun of the 2014 model, the coefficient of determination (R^2), the Root Mean Square Error (RMSE), and Willmott's index of agreement (d) [51] were computed to evaluate the goodness of the fit in the 2014 base model. For reference, a perfect fit of the simulations to the observations would have an R^2 of ± 1, an RMSE of 0, and $d = 1$, respectively.

2.4. ENVI-met output and data analysis

ENVI-met allows users to analyze simulation outputs in various ways: a) as a time series at specific receptor locations, and/or b) the spatial distribution of climatic condition at a specific elevation and time using analysis and visualization software called Leonardo, part of the ENVI-met package.

2.4.1. The green roof's impacts

Leonardo creates data-maps that can be used to compare two versions of the same environment. To evaluate the impact of the green roof, GR and NoGR versions of the same year were compared, creating a data-map displaying the difference in conditions at each grid point. The NoGR model was selected as the reference (e.g. the map shows GR – NoGR conditions).

2.4.2. The Hudson Yard's impact (comparison of 2014 GR, 2018 GR, and 2021 GR scenarios)

To evaluate microclimatic differences due to the phases of the Hudson Yards development, Leonardo was used to view differences in the spatial distribution of specific parameters, as well as their absolute values. Further visualization and analysis were performed in R version 3.6.3 (R Core Team, 2020).

2.4.3. Metrics for comparison

To compare scenarios, potential air temperature, SVF, longwave radiation (LWR), and MRT were extracted at 1:00 p.m., 9:00 p.m., and 12:00 a.m. The results were compared at 1 m elevation, hereafter referred to as "pedestrian-level," and at 23 m roughly corresponding to the elevation at the weather stations located on the JJCC roof, and thus referred to as "roof-level".

3. Results and discussion

3.1. ENVI-met simulation validation

The results of the 2014 GR simulation suggest good representation of the observed data, even during the model warm up period. Simulated air temperature and relative humidity values were compared to on-site observations at the NGR, SGR, and 11th Ave climate station locations (Fig. 3). Table 4 presents the R^2, RMSE, and Willmott's index of agreement (d). These values indicate reasonably good model performance and are similar to the reported values of ENVI-met validation results reviewed by Tsoka, Tsikaloudaki and Theodosiou [34].

3.2. The green roof's impact

This section documents the GR's ability to reduce air temperature (3.2.1) and LWR and MRT (3.2.2) over both space and time.

3.2.1. Potential air temperature

The difference between GR and NoGR (GR – NoGR) scenarios at roof-level (Fig. 4) and pedestrian-level (Fig. 5) for the entire area are shown

Table 4
Measures of the performance of the ENVI-met model field measured and simulated air temperature and relative humidity (RH) values at the height of climate station at the NGR, SGR, and Pedestrian-level at 11the Ave; R^2: coefficient of determination, RMSE: Root Mean Square error, d: Willmott's index of agreement.

	Air temperature (°C)			RH (%)		
	R^2	RMSE	d	R^2	RMSE	d
NGR	0.95	0.66	0.98	0.89	2.24	0.97
SGR	0.96	0.71	0.98	0.91	2.13	0.97
Pedestrian-level at 11th Ave	0.96	1.17	0.96	0.95	1.93	0.98

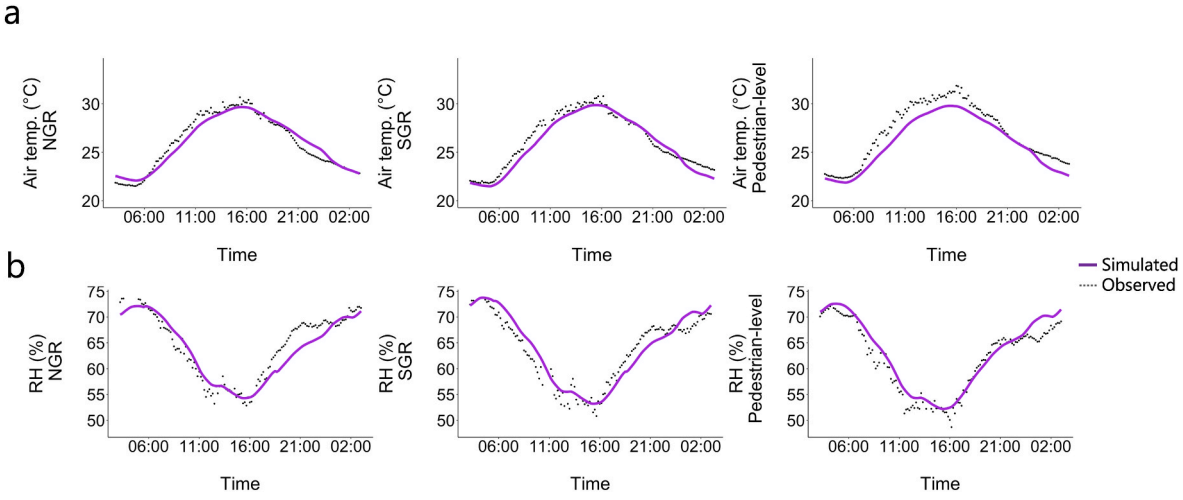

Fig. 3. Observed and simulated ENVI-met data for 7/22/2014 for NGR (left), SGR (middle), and pedestrian-level at 11th AVE (right) for: a) air temperature, and b) relative humidity (RH).

for 2014 (left), 2018 (middle), and 2021 (right) columns, respectively. The first row depicts the differences in potential air temperature at 1:00 p.m., the second row at 9:00 p.m., and the third row at 12:00 a.m. In the figures, the arrow shows true north. However, to simplify the discussion, the top of the figure is referred to as "north", the left-hand side as "west", etc. The wind direction used in the simulation was out of the lower right-hand corner of the figure (out of the true south).

At roof level (Fig. 4), the GR reduced air temperature over the NoGR condition over a geographic condition that extends to the top of the figure, and with the greatest cooling benefit on the roof area and on its downwind side (Fig. 4, top row). The cooling benefit decreased over time, however. The maximum difference was −0.75 K, −0.65 K, and −0.64 K for 2014, 2018, and 2021, respectively (reflected in blue for 2014, and turquoise for 2018 and 2021). As the air travelled over the green roof it was cooled with a "tail" stretching to the north-northeast. Because the only physical differences in the model domain between the different simulation years were the addition of the Hudson Yards buildings and a few additional street trees, the results suggest therefore that the Hudson Yards development reduced the green roof's ability to reduce air temperature over the No-GR condition.

At pedestrian level (Fig. 5), the same trends were found, but to a lesser extent. The greatest cooling was on the downwind side of the JJCC, and the maximum cooling effect was −0.52K in 2014, -0.45K in 2018, and -0.44K in 2021. Presumably due to the higher elevation of the green roof and the direction of the forcing wind, the temperature difference (or tail) was less prevalent at street level. The results are consistent with other ENVI-met simulation studies [34], which suggest that the vertical advection of air cooled by the green roof to pedestrian level is minimal, and in fact becomes negligible and less pronounced with increased vertical distance between the roof and the ground.

As depicted in Figs. 4 and 5, the green roof had no discernible effect on nighttime air temperature (9:00 p.m. and 12:00 a.m.).

The time series predictions at the receptor locations reinforce these findings. Fig. 6 compares the diurnal air temperature differences at the NGR, SGR, and pedestrian-level receptor locations (proximate location of on-site weather stations, red stars in Fig. 4) in 2014, 2018, and 2021. Though these receptors are not in the cells that displayed the maximum air temperature differences, the dampening of the green roof's cooling effect over time can be seen clearly. Comparing just the NGR receptor time series (green), 2014 yielded the greatest difference of −0.49 K, while the 2018 and 2021 air temperature differences reached a maximum of −0.43 and −0.42 K, respectively. Similar trends were observed in the SGR receptor location, with no observable effect detected at pedestrian-level receptor location. From 6:00 p.m. to 9:00 a.m., the green roof's impacts on air temperature were negligible over all three years.

These finding are consistent with our previous attempts to document air temperature differences of the JJCC green roof [28]. In that study, the difference in maximum daytime air temperature between black and green roof was found to be 1.8 °C, and the monthly median air temperature difference of the black roof relative to north green roof was about 0.4 °C in August 2013. The differences reported in the previous study were performed during construction of the green roof when one section (north) was green, and the other section (south) was black. The ENVI-met simulations compared a completely black roof to a completely greened roof. Also, the previous study compared multiple simultaneous measurements while this study simulated one specific 24-h period.

The observed and simulated reduction in air temperature over and near the green roof was expected due to its higher albedo (ability to reflect light) [52] and its ability to partition more incoming energy into latent heat flux (e.g. evapotranspiration), which does not involve a temperature change, and therefore does not contribute to a gain in

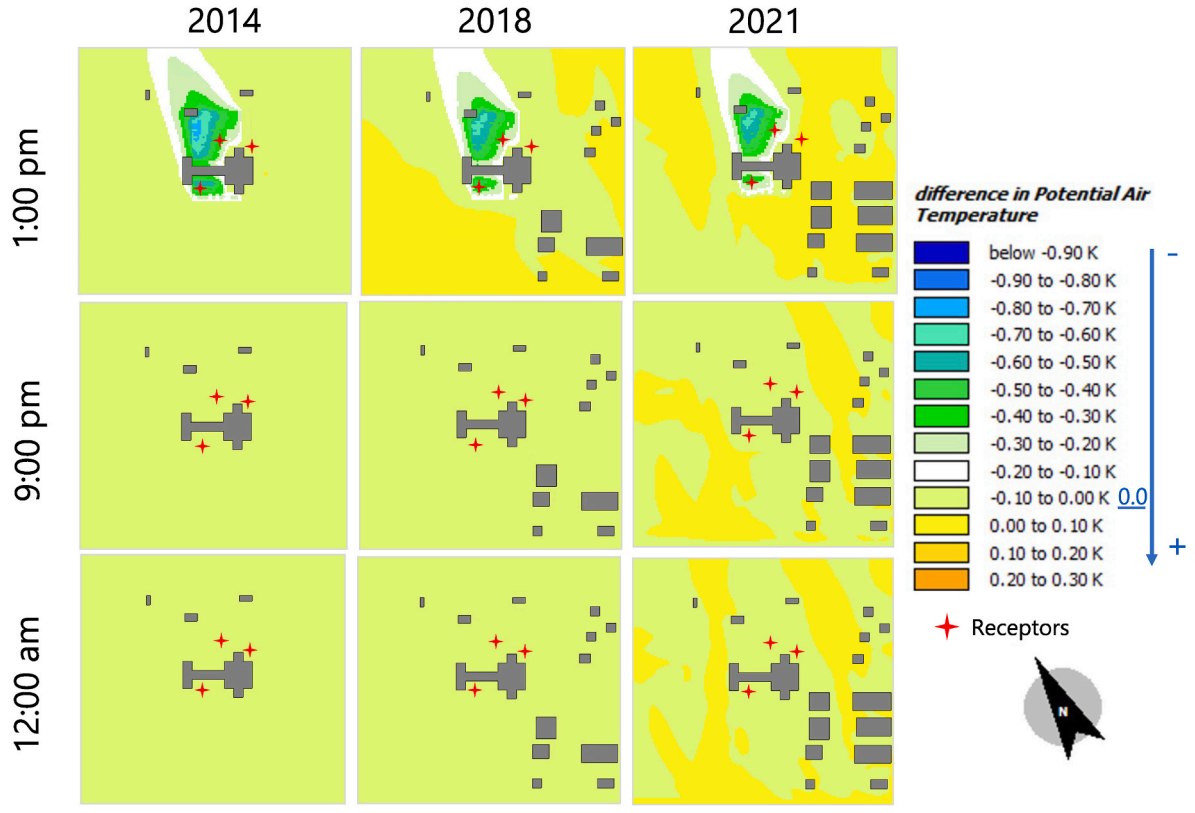

Fig. 4. Spatial air temperature difference between GR and NoGR (with NoGR as reference) at roof-level (23 m) at 1:00 p.m., 9:00 p.m. and 12:00 a.m. for 2014 (left panel), 2018 (middle panel), and 2021 (right panel) for July 22nd. Note: the color change seen elsewhere in Figs. 4 and 5 (light green and yellow) represents small, changes around zero, with the yellow being slightly positive, and the light green being slightly negative. Red stars show ENVI-met model receptor locations on NGR, SGR, and pedestrian-level at 11th Ave. (For interpretation of the references to color in this figure legend, the reader is referred to the Web version of this article.)

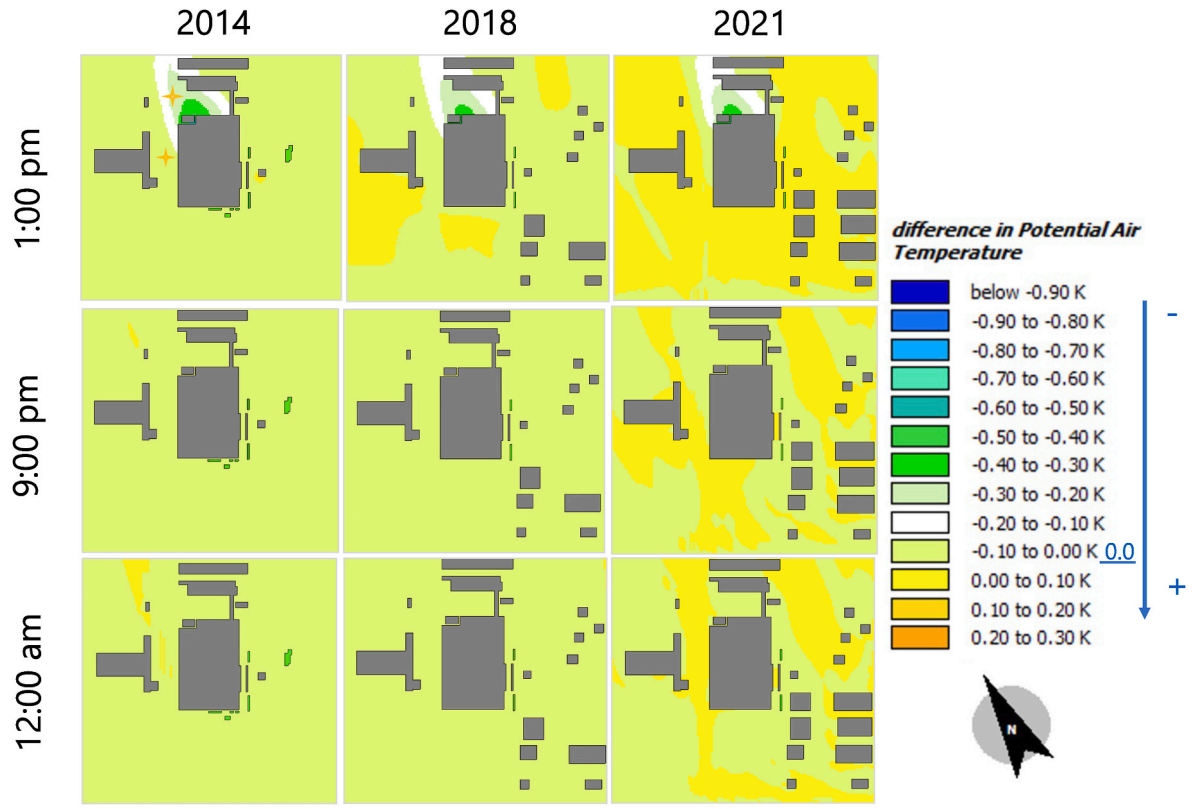

Fig. 5. Spatial air temperature difference between GR and NoGR outputs (with NoGR as reference) at pedestrian-level (1 m) at 1:00 p.m., 9:00 p.m. and 12:00 a.m. for 2014 (left panel), 2018 (middle panel), and 2021 (right panel) for July 22nd.

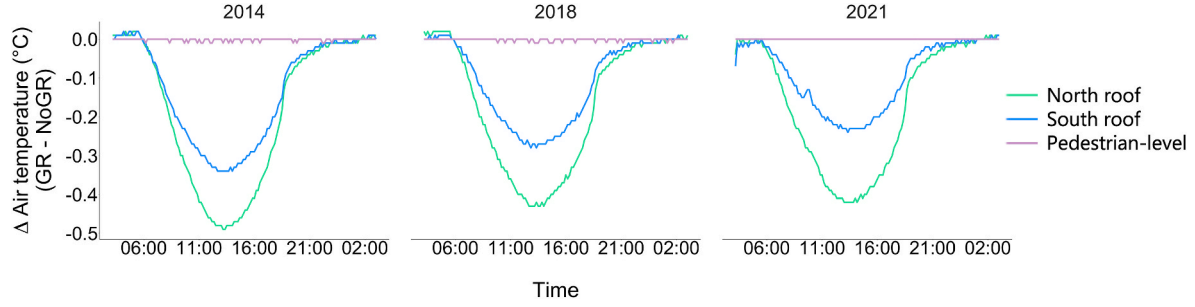

Fig. 6. The air temperature difference between GR and NoGR (GR – NoGR) scenarios at receptor locations on NGR, SGR, and pedestrian-level at 11th Ave for 2014 (left), 2018 (middle), and 2021 (right) for July 22nd.

sensible heat [28]. This air temperature reduction is crucial to a green roof's ability to mitigate UHI [53,54]. Since reflection and evapotranspiration are less significant processes at night, it is expected that nighttime differences could be negligible.

The results suggest that the greatest impact of the green roof on the street level microclimate was on its downwind side. This finding carries implications for decisions regarding green roof siting which, in places with wind directions that are fairly consistent, would be installed upwind of the regions where cooling benefits are most needed, as also suggested by other researchers [55].

3.2.2. Long Wave Radiation (LWR) and Mean Radiant Temperature (MRT)

Differences in LWR and MRT due to the GR were modest to negligible. The GR reduced LWR by a maximum of 0.21 W/m^2 at 9:00 p.m., and 0.23 W/m^2 at 12:00 a.m. in 2014. The reduction in LWR decreased further in 2018, becoming negligible in 2021 (<0.08 W/m^2). There were no observable MRT changes between GR and NoGR at 1:00 p.m., 9:00 p.m. and 12:00 a.m. for any year. Although some studies [33] indicated a reduction of MRT at roof-level due to greening, at pedestrian level lesser impacts are reported. Tsoka, Tsikaloudaki and Theodosiou [34] reported that effect of green roof's max MRT reduction is minimal if not negligible at pedestrian-level.

3.3. The Hudson Yard's impact (comparison of 2014 GR, 2018 GR, and 2021 GR scenarios)

With the GR in place, this section compares the 2014, 2018 and 2021 model results to better describe the Hudson Yard's effect on the local microclimate. The analysis focuses on SVF (3.3.1), air temperature (3.3.2), LWR (3.3.3), and MRT (3.3.4). Note that the GR was found to have no effect on SVF (compared to the no GR scenarios) in any year.

3.3.1. Urban typology, SVF spatial distribution

The pedestrian-level SVF distribution for the three models (2014 GR, 2018 GR, and 2021 GR) is shown spatially in Fig. 7a and as a box plot in

Fig. 7b. The pink and magenta SVF values (0.8–1) indicate open spaces, while the blue (0–0.3) represent dense spaces with lower sky view. The median SVF value depicted in the images was 22.5 % and 24 % higher in 2014 compared to that of 2018 and 2021, respectively. A qualitative indication of the impact of the new buildings, Fig. 7a shows a clear reduction in SVF around the new buildings in 2018 and 2021 (blue, green, yellow and orange color). These SVF differences between the scenarios are also evident in the box plot (Fig. 7b). As Hudson Yards redevelopment proceeded in 2018 and 2021, a higher urban canopy was created, decreasing the SVF, particularly to the east and southeast of the JJCC. This finding is significant because the SVF determines radiative exchanges and air temperatures, (as will be discussed below) implicating the redevelopment of Hudson Yards with microclimatic changes associated with temperature and UHI [56,57].

3.3.2. *Air temperature spatial distribution*

Spatial patterns in air temperature in 2014, 2018, 2021 and at 1:00 p.m., 9:00 p.m., and 12:00 a.m. are provided at pedestrian level in Fig. 8 and roof level in Fig. 9.

At street level, as the development progresses and the SVF decreases, the air temperatures north of the new buildings decreases, while between them and to the south, air temperatures increase slightly. For example, at pedestrian-level in the 2014 model at 1:00 p.m. (Fig. 8, first row, first column), air temperature in the Hudson Yards construction site (southeast quadrant of the figure), was 29 °C to 29.5 °C (light blue). However, when buildings are placed in that region in 2018, the temperature increases slightly to 29.5 °C to 30 °C (green) between the buildings, and to 30 °C to 30.5 °C (olive green) south of them. To the north and west sides of the JJCC, regions that were 32 °C to 32.5 °C (magenta) and above 32.5 °C (pink) in 2014, the temperature dropped further likely due to the shading provided by Hudson Yards buildings and a few new street trees, all of which block the incoming solar radiation.

At roof-level (23 m) at 1:00 p.m. (Fig. 9), the addition of Hudson Yards buildings increased air temperature over most of the study area. For example, to the south and east of the JJCC, regions that were 28.5 °C to 29 °C (dark blue) in 2014, increased to 29 °C to 29.5 °C (light blue) in 2018, with other regions 30 °C to 30.5 °C (green) to the west of the convention center. In 2021, some of the light blue is replaced with dark (still smaller region compared to that than in 2014), representing slight cooling north of the Hudson Yards building.

At pedestrian level at 9:00 p.m. and 12:00 a.m. (Fig. 8, second and third row), the new buildings initially had an overall warming effect. Temperatures to the south/southeast of JJCC increased from 2014 to 2018. For example, at 9:00 p.m., the region of 26.4 °C to 26.8 °C (orange) in 2014 extends further to the southeast into a region that was previously 26 °C to 26.4 °C (yellow) in 2014. However, temperatures dropped slightly in 2021 possibly due to higher wind speed (wind vectors shown on the maps) and turbulence generated between the new buildings.

At roof-level at 9:00 p.m. (Fig. 9, middle), the buildings had a cooling effect, with the temperature falling from 26.4 °C to 26.8 °C (orange) to 26 °C to 26.4 °C (yellow) to the west, and from 26.8 °C to 27.2 °C (red) to 26.4 °C to 26.8 °C (orange) on the north side of the simulation. Similar trends were observed at 12:00 a.m., the addition of the Hudson Yards buildings in 2018 added orange (23.2 °C to 23.9 °C) southwest of JJCC where red (23.9 °C to 24.6 °C) was predominant in 2014.

The impact of the new buildings on diurnal temperatures is further demonstrated in Fig. 10 for the three receptor locations. The greatest differences are at the peak, and in all three cases, the lowest temperature is in 2014, the highest in 2018, with 2021 intermediate.

3.3.3. *Longwave radiation (LWR) spatial distribution*

Fig. 11a depicts spatial patterns in pedestrian-level LWR at 9:00 p.m. (first row) and 12:00 a.m. (second row) with Fig. 11b and c depicting the same information in box plots. As indicated by light blue, green, and white in Fig. 11a, during night-time hours at pedestrian-level (9:00 p.m. and 12:00 a.m.), LWR was lower in areas with low SVF in between the Hudson Yards buildings compared to other regions with higher SVF. At 12:00 a.m. (Fig. 11, second row) there is greater variability in LWR in between the Hudson Yards buildings evident in both 2018 and 2021. Higher building density results in greater emissions of longwave radiation due to greater building surface area and higher thermal mass relative to the regions with lower building density. The increased intensity of LWR is also evident in box plots (Fig. 11b).

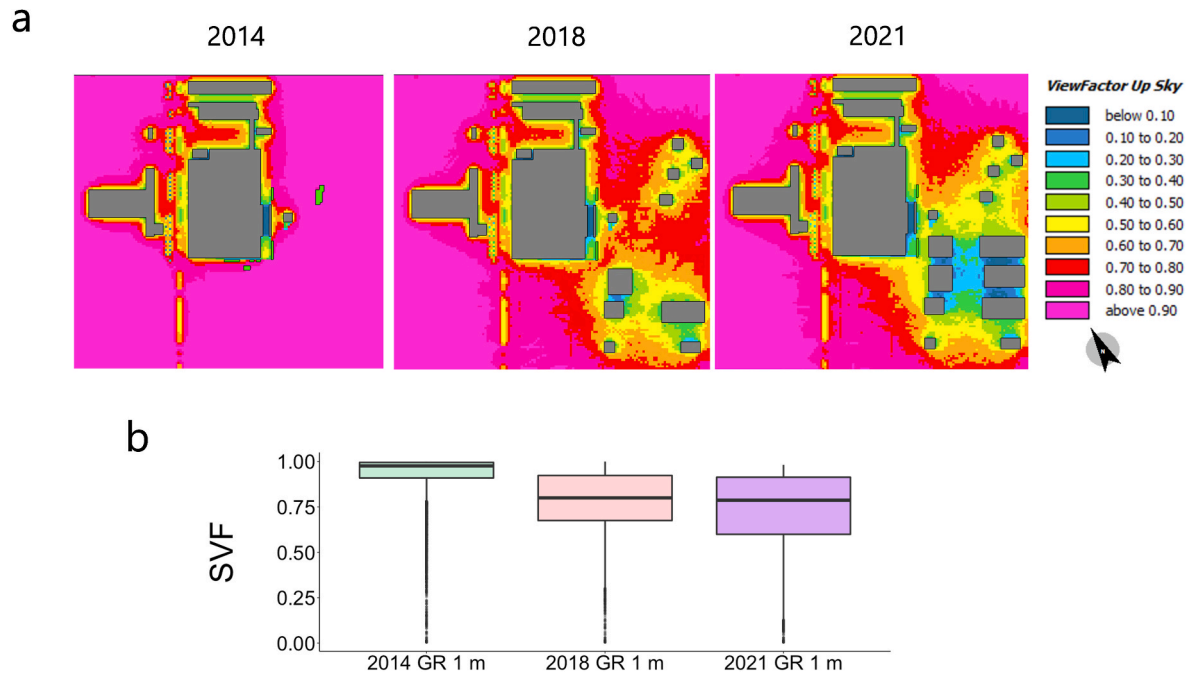

Fig. 7. Sky view factor (SVF) distribution at pedestrian-level: a) simulation image for 2014 (left), 2018 (middle), and 2021 (right) and b) box plot comparing the SVF distributions.

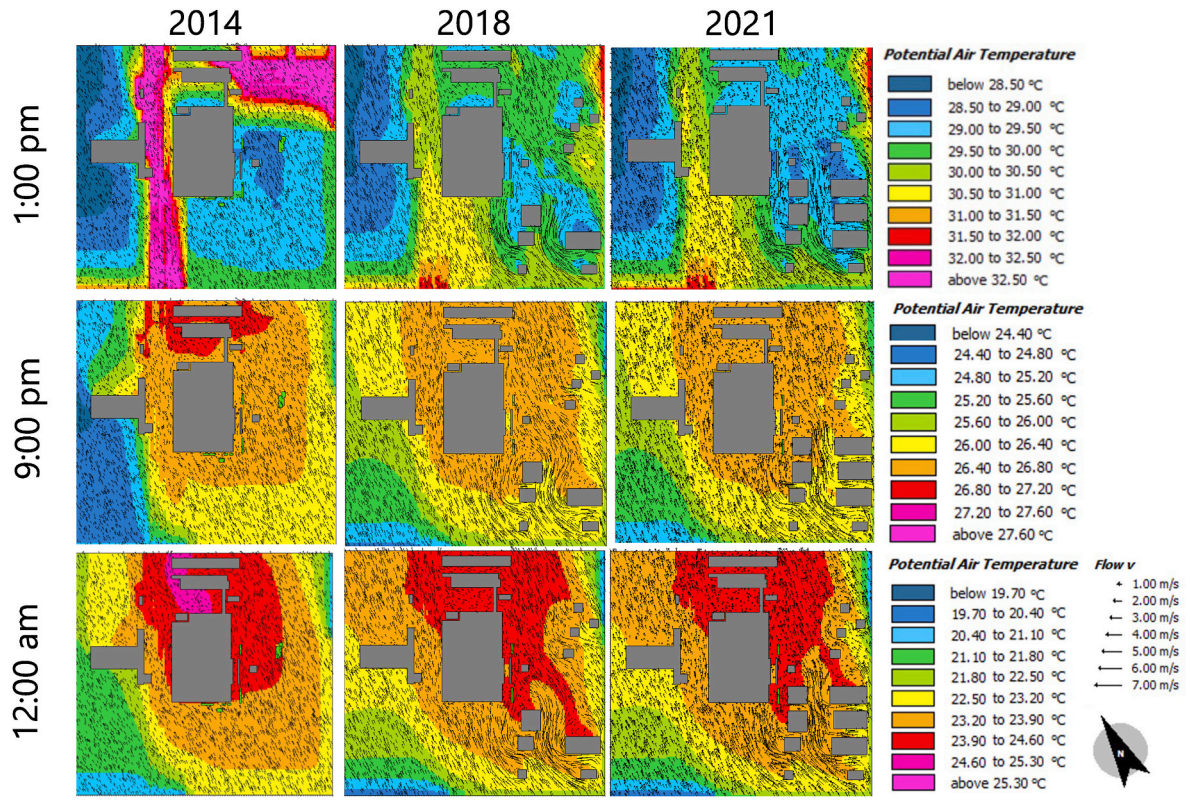

Fig. 8. Air temperature: a) distribution at pedestrian-level for 2014 (left), 2018 (middle), and 2021(right) scenarios at 1:00 p.m., 9:00 p.m., and 12:00 a.m., also shown are wind vectors, b-d) box plot at 1:00 p.m., 9:00 p.m., and 12:00 a.m. respectively.

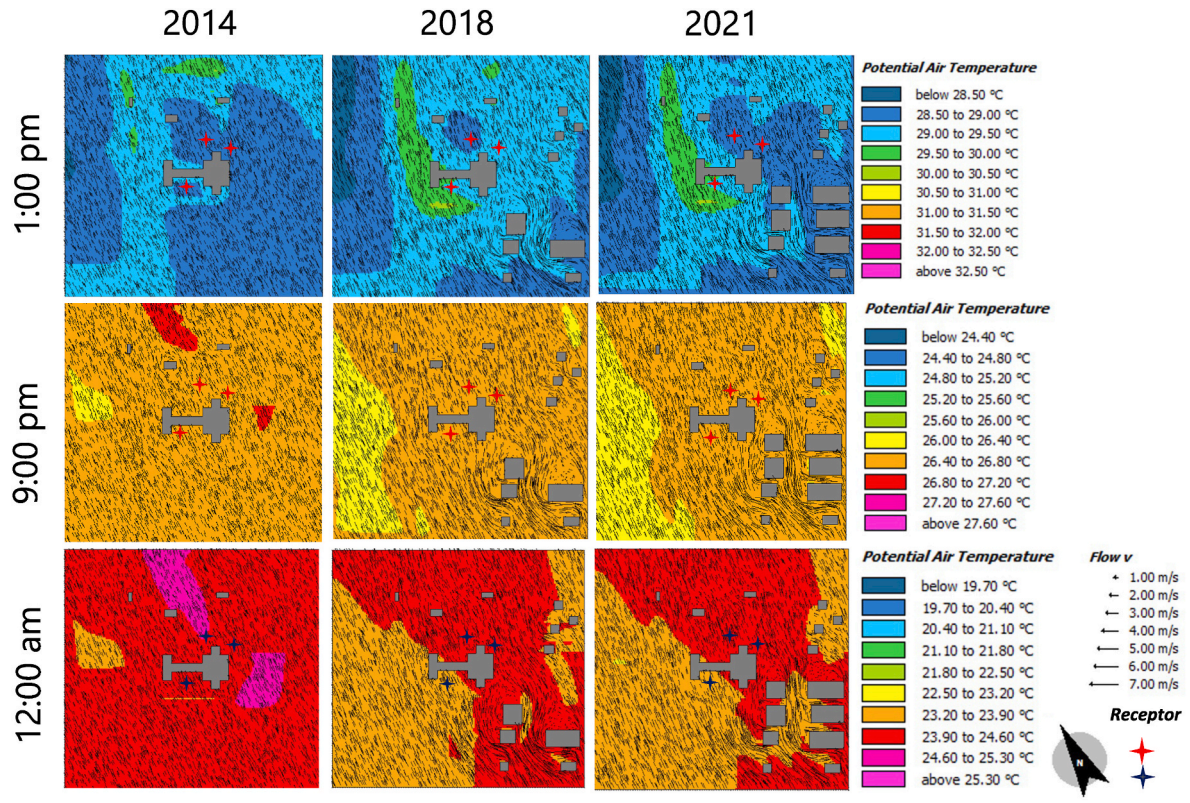

Fig. 9. Air temperature: a) distribution at roof-level for 2014 (left), 2018 (middle), and 2021(right) scenarios at 1:00 p.m., 9:00 p.m., and 12:00 a.m., b-d) box plot at 1:00 p.m., 9:00 p.m., and 12:00 a.m. respectively. Red and blue stars show ENVI-met model receptor locations on NGR, SGR, and pedestrian-level at 11th Ave. (For interpretation of the references to color in this figure legend, the reader is referred to the Web version of this article.)

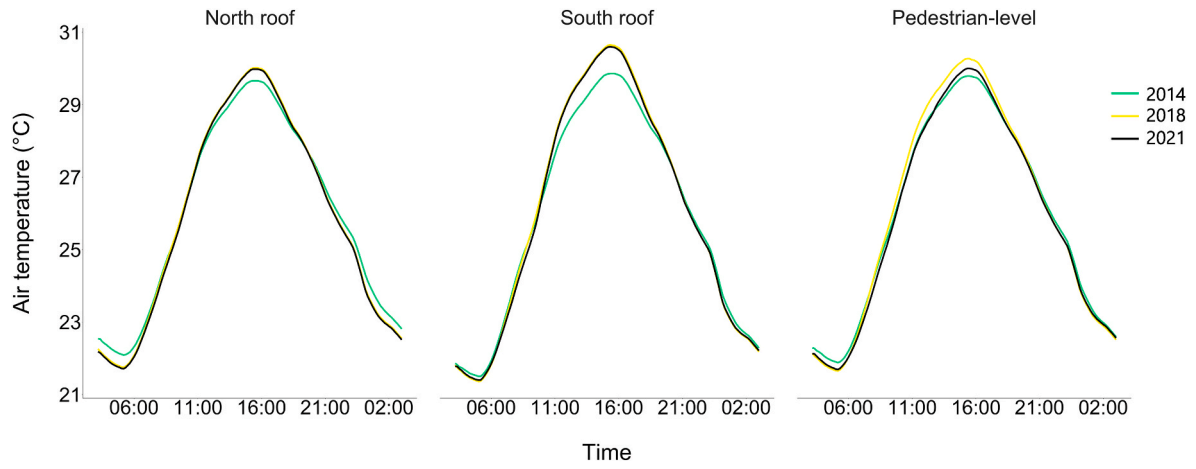

Fig. 10. Comparison of air temperature for 2014 GR (green), 2018 GR (yellow) and 2021GR (black), over the course of simulation at receptor locations on NGR (left), SGR (middle), and pedestrian-level at 11th Ave (left) for July 22nd. (For interpretation of the references to color in this figure legend, the reader is referred to the Web version of this article.)

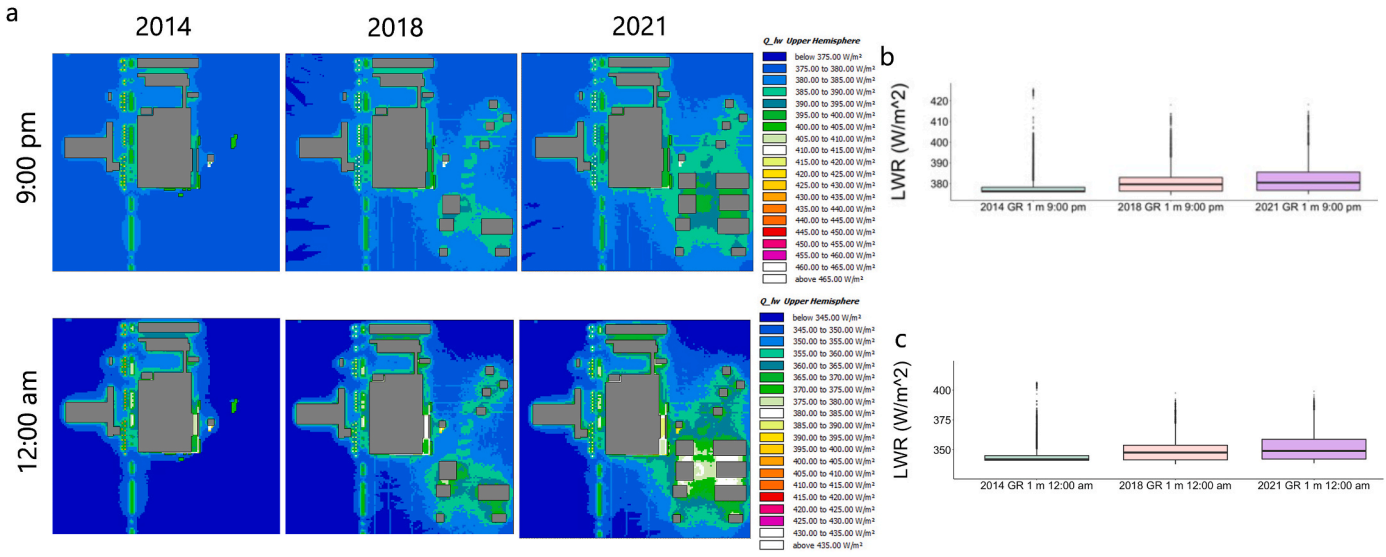

Fig. 11. Long wave radiation (LWR) at pedestrian level: a) spatial distribution for 2014 (left), 2018 (middle) and 2021 (right) at 9:00 p.m. and 12:00 a.m.: b-c) box plot at 9:00 p.m., and 12:00 a.m. respectively.

3.3.4. Mean radiant temperature (MRT) distribution

Figs. 12 and 13 display the spatial distribution and box plots of MRT at pedestrian-level and roof-level, respectively, for the three models (2014 GR, 2018 GR, and 2021 GR).

At 1:00 p.m., in the 2014 model at pedestrian-level (Fig. 12a, top row), MRT was >63 °C (black and gray color), throughout the simulated environment and extending into the Hudson Yards construction site (lower right quadrant). When the buildings were added in 2018, there was a decrease in MRT between the buildings, ranging from 45.5 °C to 48 °C (light green) and 43 °C to 45.5 °C (light blue). In 2021, as more buildings were added, these regions showed even lower MRT values between the buildings and to their north, ranging from 40.5 °C to 43 °C (dark blue), 43 °C to 45.5 °C (light blue), and 60.5 °C to 63 °C (pink). These differences are also evident in the box plots. The median value of MRT at the pedestrian-level in 2018 was 0.14 °C lower than 2014, and in 2021 it was 1.65 °C lower than 2014.

By contrast, the trends at 9:00 p.m. and 12:00 a.m. were opposite to those shown at 1:00 p.m., with higher MRT values observed in both 2018 and 2021 compared to 2014. These differences are also evident in the box plots. For example, at 12:00 a.m., the median MRT in 2018 was 0.65 °C higher than 2014, and in 2021 it was 0.74 °C higher than 2014. Similar trends of MRT were found at the roof-level (Fig. 13).

At 1:00 p.m., when the sunlight is present, the most obvious decrease in MRT occurs in the shadows cast by the buildings. This reduction in MRT is considered to play an important role in reducing heat stress caused by high direct solar radiation [58]. There is also apparent MRT reduction in the area surrounding the JJCC at 1:00 p.m., which is likely also linked to shading. Throughout the day, as the sun rises and moves across the sky, the movement of shadows cast by the buildings create shaded areas on the ground and structures, limiting direct sunlight exposure, decreasing the amount of direct solar radiation experienced by the surfaces during the day, and reducing the temperature of that surface relative to the surfaces that encounter day-long sunlight [59].

The shading profile throughout the daylight hours for 2021 at 1:00 m height can be seen in Fig. 14. During the day, the movement of shadows was observed to pass over the area that experienced a decrease in MRT relative to the region not reached by the shadow. At night, however, the highest intensity of MRT was observed between the buildings of Hudson Yards with lower SVF values. This finding is consistent with the notion that higher building density and concentration of built surfaces increase

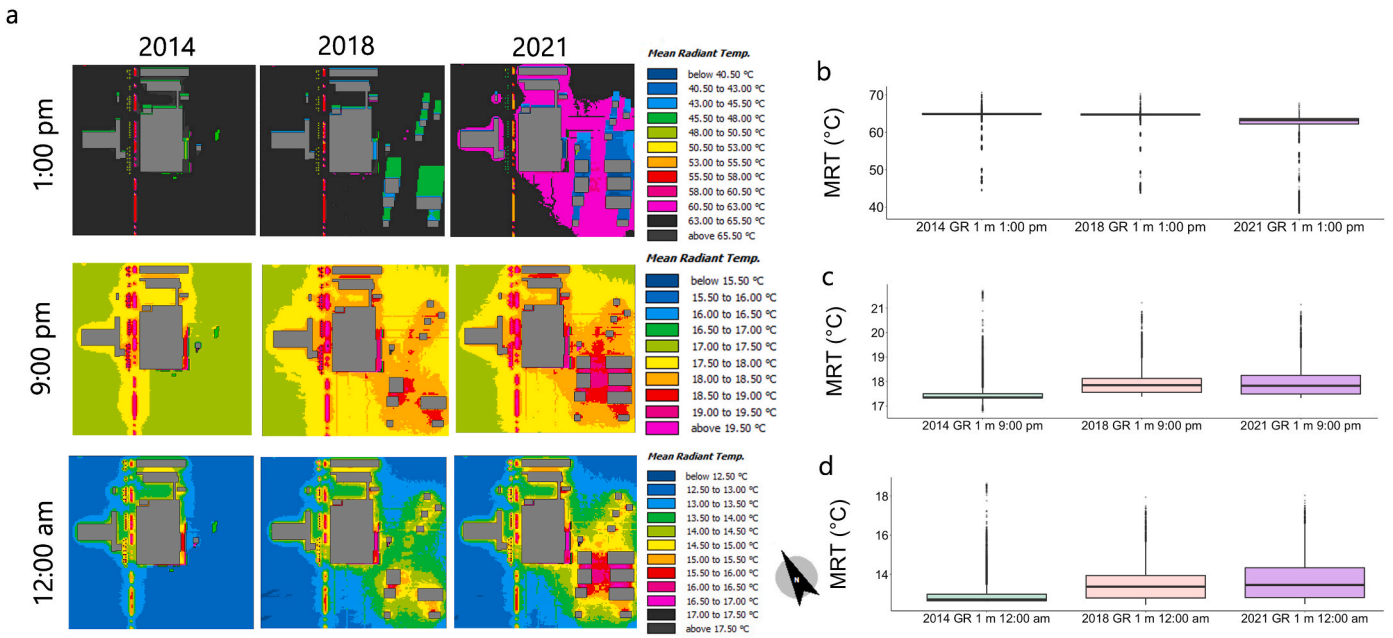

Fig. 12. Mean radiant temperature: distribution at pedestrian-level for 2014 (left), 2018 (middle), and 2021 (right) at 1:00 p.m., 9:00 p.m. and 12:00 a.m. and b-d) at 1:00 p.m., 9:00 p.m., and 12:00 a.m. respectively.

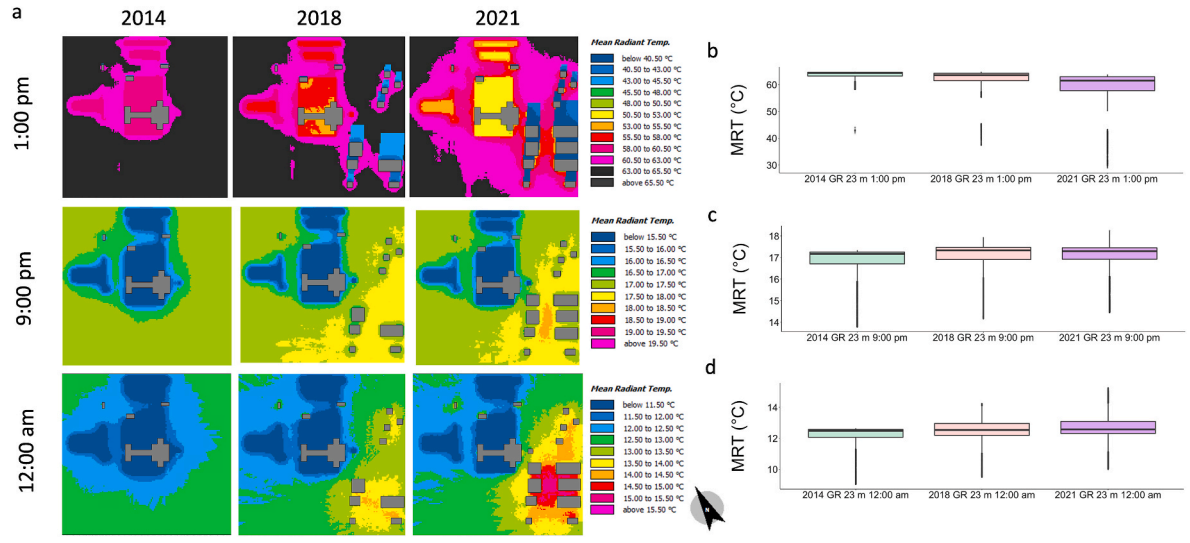

Fig. 13. Mean radiant temperature: distribution at roof-level for 2014 (left), 2018 (middle), and 2021 (right) at 1:00 p.m., 9:00 p.m. and 12:00 a.m. and b-d) box plots at 1:00 p.m., 9:00 p.m., and 12:00 a.m. respectively.

the capacity of an area for trapping heat. Conversely, areas with high SVF dissipate heat better than those with low SVF. Moreover, the amount of surface area radiating heat is also larger with a higher building density.

3.4. Synthesis

The addition of the Hudson Yards buildings created a lower SVF. During the day, the lower SVF offered more shading, reduced solar radiation exposure at the pedestrian-level, and generally reduced air temperature and MRT in the building's shadows. The new buildings block the shortwave radiation during the day contributes, reducing daytime MRT. In addition, the increase in the size and density of the flow vectors in Figs. 8 and 9 (with air temperature) indicate higher wind speed and turbulent flow at the corners of, and between the buildings. These results suggest that the addition of the Hudson Yards buildings in 2018 and 2021 reduced MRT during the daylight hours (Figs. 11 and 12), suggesting that during the day, pedestrians on the ground likely benefitted from the shade.

However, by contrast, the addition of the Hudson Yards buildings and the reduction in SVF from 2014 to 2018, and from 2018 to 2021 possibly led to increase LWR, MRT at night. The more pronounced increase in MRT was at pedestrian-level, as shown in Fig. 12. Although the Hudson Yards buildings provide some areas with reduced access to the solar radiation during the day, it is evident that the narrow and tall urban canyon traps more radiation and restricts outgoing longwave radiation at night due to the addition of more constructed surfaces blocking the cool night sky, and an increase of material with a higher storage capacity and emittance of LWR. Higher intensities of LWR and hence MRT in the areas around the building indicate a worsening of the

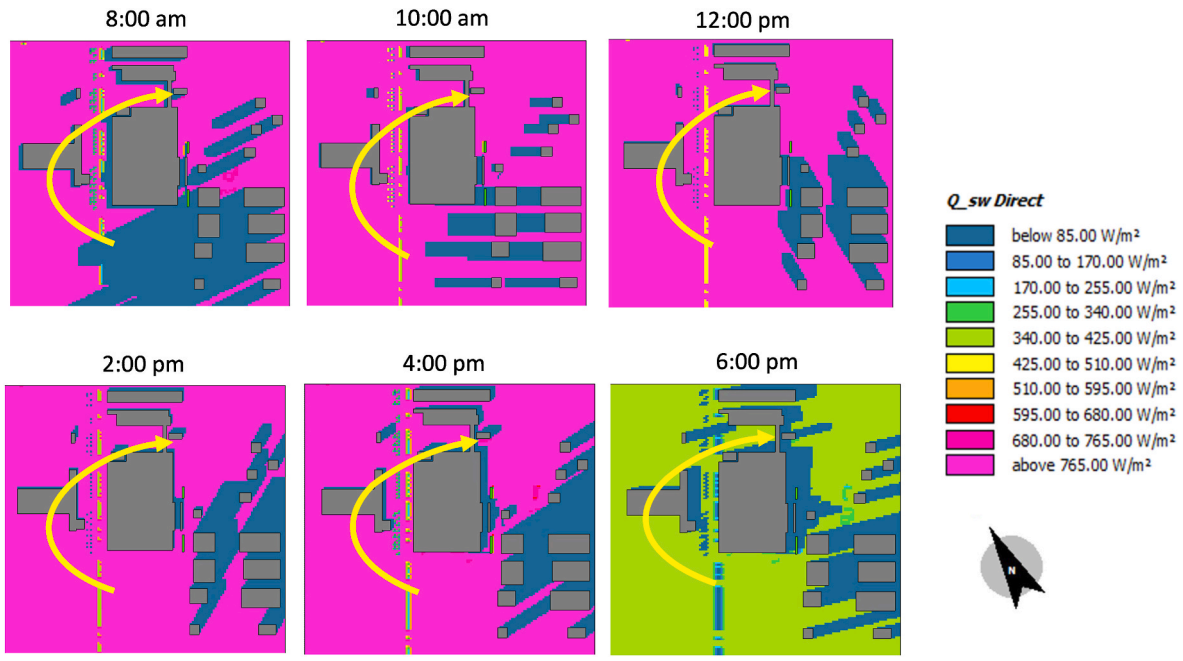

Fig. 14. Direct solar radiation at 1 m height for 8:00 a.m., 10:00 a.m., 12:00 p.m., 2:00 p.m., 4:00 p.m., and 6:00 p.m. As illustrated by the yellow drawn arrow, the path of the Sun overhead, and the placement of the buildings create shadows that pass from the South side of the environment clockwise to the east, providing shade to those areas over the course of a day. (For interpretation of the references to color in this figure legend, the reader is referred to the Web version of this article.)

nighttime UHI, compared to 2014, before the Hudson Yards development was begun.

4. Conclusions

This study demonstrated how the JJCC green roof and the Hudson Yards redevelopment (not built, partly built, fully built) determined their shared neighborhood microclimate. Simulations of these models (2014, 2018, and 2021) with the green roof (GR) were compared with the simulations of models without the green roof (NoGR). This study further extended the work of Alvizuri, Cataldo, Smalls-Mantey and Montalto [41] and Smalls-Mantey and Montalto [28] by investigating the connection between the JJCC green roof and its surrounding complex and dynamic urban landscape.

The addition of the JJCC green roof in 2014 scenario reduced air temperature compared to the NoGR condition that preceded it (maximum reduction of 0.75 K, at 1:00 p.m.). However, the green roof's ability to mitigate UHI through reduced air temperature was then reduced over time as the Hudson Yards redevelopment proceeded. Since there were no observable MRT differences between the GR and NoGR scenarios, the remainder of the analysis focuses on the climatological impact of the Hudson Yards buildings, comparing the 2014, 2018, and 2021 green roof scenarios.

Overall, the ENVI-met simulations demonstrate changes in all microclimatic variables (e.g., air temperature, LWR, MRT), over time, as the Hudson Yards project proceeded from its conception (2014) to its completion (2021). The addition of the Hudson Yards buildings created lower SVF, and during the daytime provided shading from direct solar radiation and improved MRT. However, in 2018 and 2021 the new buildings incrementally trapped radiation at night, resulting in higher MRT.

The analysis has several limitations. The research team had incomplete access to construction plans and specifications drawings for the structures present in the study area. Customized material properties were specified where possible, but in some cases (including soil temperature, moisture content, and the temperature of the Hudson River) the use of default materials was necessary. All material properties, (customized and default), were held constant across all simulations. Assumptions regarding material properties such as heat capacity and thermal conductivity could influence the heat exchange between the surface and atmosphere, as could assumptions regarding the roughness length, but the research team did not have the resources to conduct a full sensitivity analysis to evaluate the scale of impact of these assumptions. A preliminary analysis of air temperature gradients relative to the location of the Lincoln Tunnel vents was conducted and determined no effect, but a more elaborate study could be conducted as a follow up study. The research team also lacked the computational resources (and associated economic resources) to conduct simulations that exceeded 24 h, limiting our ability to study longer-term trends and variations, and to analyze spatial differences in the results at time slices other than13:00 p.m., 21 p.m., and midnight.

Despite these limitations, the findings provide insights into the microclimate of complex urban environments and landscapes. Deeper insights into the complex and dynamic relationship between urban green spaces and the built environment can better equip urban designers to design more sustainable spaces. Understanding the intricate connection between urban nature-based solutions and the built environment allows planners and decision-makers to enhance the adaptive capacity of cities in the face of climate change and prepare to withstand and recover from climate-related disruptions. Ongoing work seeks to characterize, through monitoring, the microclimate of new green spaces (e.g., a rooftop farm, orchard, and food forest) introduced into this section of NYC since completion of the present study.

Funding

This research was funded principally by the Jacob K. Javits Convention Center, with additional support by the National Oceanic and Atmospheric Administration (NOAA) through Supporting Regional Implementation of Integrated Climate Resilience: Consortium for Climate Risks in the Urban Northeast (CCRUN) (NA15OAR4310147).

CRediT authorship contribution statement

Bita Alizadehtazi: Writing – review & editing, Writing – original draft, Visualization, Validation, Software, Methodology, Formal analysis, Data curation, Conceptualization. **Julian Stolper:** Writing – review & editing, Writing – original draft, Visualization, Software, Methodology, Conceptualization. **Katelyn Singh:** Writing – review & editing, Writing – original draft. **Franco A. Montalto:** Writing – review & editing, Writing – original draft, Supervision, Resources, Project administration, Methodology, Investigation, Funding acquisition, Conceptualization.

Declaration of competing interest

The authors declare that they have no known competing financial interests or personal relationships that could have appeared to influence the work reported in this paper.

Data availability

Data will be made available on request.

Acknowledgments

The authors acknowledge contributions to this paper by Dr. Lauren Smalls-Mantey and Dr. Leena Shevade.

Appendix A. Supplementary data

Supplementary data to this article can be found online at https://doi.org/10.1016/j.buildenv.2023.111113.

References

[1] T.R. Oke, City size and the urban heat island, Atmos. Environ. 7 (8) (1973) 769–779.
[2] M. Santamouris, Analyzing the heat island magnitude and characteristics in one hundred Asian and Australian cities and regions, Sci. Total Environ. 512 (2015) 582–598.
[3] D. Armson, P. Stringer, A. Ennos, The effect of tree shade and grass on surface and globe temperatures in an urban area, Urban For. Urban Green. 11 (3) (2012) 245–255.
[4] P. Ramamurthy, E. Bou-Zeid, Heatwaves and urban heat islands: a comparative analysis of multiple cities, J. Geophys. Res. Atmos. 122 (1) (2017) 168–178.
[5] R.S. Kovats, S. Hajat, Heat stress and public health: a critical review, Annu. Rev. Publ. Health 29 (2008) 41–55.
[6] S. Savić, V. Marković, I. Šećerov, D. Pavić, D. Arsenović, D. Milošević, D. Dolinaj, I. Nagy, M. Pantelić, Heat wave risk assessment and mapping in urban areas: case study for a midsized Central European city, Novi Sad (Serbia), Nat. Hazards 91 (3) (2018) 891–911.
[7] A. Tzavali, J.P. Paravantis, G. Mihalakakou, A. Fotiadi, E. Stigka, Urban heat island intensity: a literature review, Fresenius Environ. Bull. 24 (12b) (2015) 4537–4554.
[8] L. Guo, R. Liu, C. Men, Q. Wang, Y. Miao, Y. Zhang, Quantifying and simulating landscape composition and pattern impacts on land surface temperature: a decadal study of the rapidly urbanizing city of Beijing, China, Sci. Total Environ. 654 (2019) 430–440.
[9] E. Morini, A.G. Touchaei, B. Castellani, F. Rossi, F. Cotana, The impact of albedo increase to mitigate the urban heat island in Terni (Italy) using the WRF model, Sustainability 8 (10) (2016) 999.
[10] I.D. Stewart, Why should urban heat island researchers study history? Urban Clim. 30 (2019) 100484.
[11] M.P. Heris, A. Middel, B. Muller, Impacts of form and design policies on urban microclimate: assessment of zoning and design guideline choices in urban redevelopment projects, Landsc. Urban Plann. 202 (2020) 103870.
[12] H. Liu, B. Huang, Q. Zhan, S. Gao, R. Li, Z. Fan, The influence of urban form on surface urban heat island and its planning implications: evidence from 1288 urban clusters in China, Sustain. Cities Soc. 71 (2021) 102987.
[13] I.D. Stewart, A systematic review and scientific critique of methodology in modern urban heat island literature, Int. J. Climatol. 31 (2) (2011) 200–217.
[14] I.D. Stewart, T.R. Oke, Local climate zones for urban temperature studies, Bull. Am. Meteorol. Soc. 93 (12) (2012) 1879–1900.
[15] J. Cao, W. Zhou, J. Wang, X. Hu, W. Yu, Z. Zheng, W. Wang, Significant increase in extreme heat events along an urban–rural gradient, Landsc. Urban Plann. 215 (2021) 104210.
[16] T.R. Oke, Boundary Layer Climates, Routledge, 2002.
[17] B. Deevi, F.A. Chundeli, Quantitative outdoor thermal comfort assessment of street: a case in a warm and humid climate of India, Urban Clim. 34 (2020) 100718.
[18] M. Bruse, H. Fleer, Simulating surface–plant–air interactions inside urban environments with a three dimensional numerical model, Environ. Model. Software 13 (3–4) (1998) 373–384.
[19] F. Salata, I. Golasi, D. Petitti, E. de Lieto Vollaro, M. Coppi, A. de Lieto Vollaro, Relating microclimate, human thermal comfort and health during heat waves: an analysis of heat island mitigation strategies through a case study in an urban outdoor environment, Sustain. Cities Soc. 30 (2017) 79–96.
[20] X. Yang, L. Zhao, M. Bruse, Q. Meng, Evaluation of a microclimate model for predicting the thermal behavior of different ground surfaces, Build. Environ. 60 (2013) 93–104.
[21] A. Motazedian, P. Leardini, Impact of green infrastructures on urban microclimates: a critical review of data collection methods, in: H. Skates (Ed.), 46th Annual Conference of the Architectural Science Association, Griffith University, Department of Architecture, Brisbane, Australia, 2012.
[22] B. Alizadehtazi, P.L. Gurian, F.A. Montalto, Impact of successive rainfall events on the dynamic relationship between vegetation canopies, infiltration, and recharge in engineered urban green infrastructure systems, Ecohydrology 13 (2) (2020) e2185.
[23] B. Alizadehtazi, P.L. Gurian, F.A. Montalto, Observed variability in soil moisture in engineered urban green infrastructure systems and linkages to ecosystem services, J. Hydrol. 590 (2020) 125381.
[24] B. Alizadehtazi, K. DiGiovanni, R. Foti, T. Morin, N.H. Shetty, F.A. Montalto, P. L. Gurian, Comparison of observed infiltration rates of different permeable urban surfaces using a cornell sprinkle infiltrometer, J. Hydrol. Eng. 21 (7) (2016) 06016003.
[25] L.J. Shevade, L.J. Lo, F.A. Montalto, Numerical 3D model development and validation of curb-cut inlet for efficiency prediction, Water 12 (6) (2020) 1791.
[26] L.J. Shevade, F.A. Montalto, Forensic investigation of four monitored green infrastructure inlets, Water 13 (13) (2021) 1787.
[27] M.R. De Sousa, F.A. Montalto, P. Gurian, Evaluating green infrastructure stormwater capture performance under extreme precipitation, J. Extreme Events 3 (2) (2016) 1650006.
[28] L. Smalls-Mantey, F. Montalto, The seasonal microclimate trends of a large scale extensive green roof, Build. Environ. (2021) 107792.
[29] K. DiGiovanni, F. Montalto, S. Gaffin, C. Rosenzweig, Applicability of classical predictive equations for the estimation of evapotranspiration from urban green spaces: green roof results, J. Hydrol. Eng. 18 (1) (2013) 99–107.
[30] B. Alizadehtazi, F.A. Montalto, Precipitation and soil moisture data in two engineered urban green infrastructure facilities in New York City, Data Brief 32 (2020) 106225.
[31] B. Alizadehtazi, S. Woerdeman, K. Tangtrakul, A. Gussenhoven, N. Mostafavi, F. A. Montalto, Recruiting, paying, and evaluating the experiences of civic scientists studying urban park usage during the beginning of the COVID-19 pandemic, Front. Sustain. Cities 4 (2022) 709968.
[32] J. Tyler, A. Bendix, Hudson Yards Is the Most Expensive Real-Estate Development in US History. Here's what It's like inside the $25 Billion Neighborhood, Business Insider, 2019.
[33] U. Berardi, The outdoor microclimate benefits and energy saving resulting from green roofs retrofits, Energy Build. 121 (2016) 217–229.
[34] S. Tsoka, A. Tsikaloudaki, T. Theodosiou, Analyzing the ENVI-met microclimate model's performance and assessing cool materials and urban vegetation applications–A review, Sustain. Cities Soc. 43 (2018) 55–76.
[35] C. Ciacci, N. Banti, V. Di Naso, F. Bazzocchi, Green strategies for improving urban microclimate and air quality: a case study of an Italian industrial district and facility, Build. Environ. 244 (2023) 110762.
[36] A. Liu, X. Ma, M. Du, M. Su, B. Hong, The cooling intensity of green infrastructure in local climate zones: a comparative study in China's cold region, Urban Clim. 51 (2023) 101631.
[37] X. Zheng, F. Kong, H. Yin, A. Middel, S. Yang, H. Liu, J. Huang, Green roof cooling and carbon mitigation benefits in a subtropical city, Urban For. Urban Green. 86 (2023) 128018.
[38] J. Iaria, T. Susca, Analytic Hierarchy Processes (AHP) evaluation of green roof-and green wall-based UHI mitigation strategies via ENVI-met simulations, Urban Clim. 46 (2022) 101293.
[39] Y. Feng, J. Wang, W. Zhou, X. Li, X. Yu, Evaluating the cooling performance of green roofs under extreme heat conditions, Front. Environ. Sci. 10 (2022) 874614.
[40] F. Balany, N. Muttil, S. Muthukumaran, M.S. Wong, A.W. Ng, Studying the effect of blue-green infrastructure on microclimate and human thermal comfort in melbourne's central business district, Sustainability 14 (15) (2022) 9057.
[41] J. Alvizuri, J. Cataldo, L. Smalls-Mantey, F. Montalto, Green roof thermal buffering: insights derived from fixed and portable monitoring equipment, Energy Build. 151 (2017) 455–468.
[42] M. Kimmelman, Hudson Yards Is Manhattan's Biggest, Newest, Slickest Gated Community. Is This the Neighborhood New York Deserves? The New York Times, nytimes.com, 2019.
[43] F. Salata, I. Golasi, R. de Lieto Vollaro, A. de Lieto Vollaro, Urban microclimate and outdoor thermal comfort. A proper procedure to fit ENVI-met simulation outputs to experimental data, Sustain. Cities Soc. 26 (2016) 318–343.
[44] J. Yang, X. Hu, H. Feng, S. Marvin, Verifying an ENVI-met simulation of the thermal environment of Yanzhong square park in shanghai, Urban For. Urban Green. 66 (2021) 127384.
[45] Knowledge base: total model height. https://envi-met.info/documents/onlinehelpv3/hs780.htm, 2020.
[46] V.G.L.-A.h.m. model. https://envi-met.info/doku.php?id=kb:verticalgrid, 2020, 2020.

[47] WMO, Guide to Meteorological Instruments and Methods of Observation (WMO-No. 8, Updated 2021)..
[48] NYC Street Tree Map. https://tree-map.nycgovparks.org/tree-map, 2020.
[49] The Skyscrape Center - Council on Tall Buildings and Urban Habitat, 30 Hudson Yards, 2020. https://www.skyscrapercenter.com/building/30-hudson-yards/13325.
[50] Council on Tall Buildings and Urban Habitat, 2020. www.skyscrapercenter.com.
[51] C.J. Willmott, D.E. Wicks, An empirical method for the spatial interpolation of monthly precipitation within California, Phys. Geogr. 1 (1) (1980) 59–73.
[52] K.R. Smith, P.J. Roebber, Green roof mitigation potential for a proxy future climate scenario in Chicago, Illinois, J. Appl. Meteorol. Climatol. 50 (3) (2011) 507–522.
[53] M. Santamouris, Cooling the cities–a review of reflective and green roof mitigation technologies to fight heat island and improve comfort in urban environments, Sol. Energy 103 (2014) 682–703.
[54] H. Akbari, C. Cartalis, D. Kolokotsa, A. Muscio, A.L. Pisello, F. Rossi, M. Santamouris, A. Synnefa, N.H. Wong, M. Zinzi, Local climate change and urban heat island mitigation techniques – the state of the art, J. Civ. Eng. Manag. 22 (1) (2016) 1–16.
[55] G. Zhang, B.-J. He, Z. Zhu, B.J. Dewancker, Impact of morphological characteristics of green roofs on pedestrian cooling in subtropical climates, Int. J. Environ. Res. Publ. Health 16 (2) (2019) 179.
[56] T.R. Oke, Canyon geometry and the nocturnal urban heat island: comparison of scale model and field observations, J. Climatol. 1 (3) (1981) 237–254.
[57] E. Johansson, Influence of urban geometry on outdoor thermal comfort in a hot dry climate: a study in Fez, Morocco, Build. Environ. 41 (10) (2006) 1326–1338.
[58] A. Ahmadi Venhari, M. Tenpierik, M. Taleghani, The role of sky view factor and urban street greenery in human thermal comfort and heat stress in a desert climate, J. Arid Environ. 166 (2019) 68–76.
[59] D. Alobaydi, M.A. Bakarman, B. Obeidat, The impact of urban form configuration on the urban heat island: the case study of Baghdad, Iraq, Procedia Eng. 145 (2016) 820–827.